Pore Size Distribution of Porous Glasses: A Test of the Independent Pore Model

Susana Figueroa-Gerstenmaier,[†] Josep Bonet Avalos,[†] Lev D. Gelb,[‡] Keith E. Gubbins,[§] and Lourdes F. Vega*[,†]

Departament d'Enginyeria Química, ETSEQ, Universitat Rovira i Virgili, Avinguda dels Països Catalans 26, Campus Sescelades, 43007 Tarragona, Spain, Department of Chemistry, Washington University in St. Louis, St. Louis, Missouri 63130-1134, and Department of Chemical Engineering, North Carolina State University, Raleigh, North Carolina 27695-7905

Received April 23, 2003. In Final Form: July 22, 2003

Using the Kierlik and Rosinberg fundamental measure theory, we test the density functional theory method for determination of pore size distributions from adsorption data for porous glasses. The glasses chosen for study are model glasses prepared by a quench molecular dynamics method that mimics the experimental synthesis process and are completely characterized at the molecular level. The density functional method involves two approximations: (a) the glasses can be regarded as made up of a distribution of nonconnected pores of simple geometry, which we refer to as the *independent pore model*, and (b) the adsorption isotherms for these nonconnected pores can be described by the density functional theory. Using simulated adsorption isotherm data for the glasses and adsorption isotherms for the pores of simple geometry calculated by the density functional theory, a regularization method is used to determine the pore size distribution from the adsorption data. These calculated pore size distributions, as well as the adsorption isotherms for the materials, are compared with the exact geometric pore size distributions for the material and with the simulated isotherms. Both slit-shaped and cylindrical pores are used in the density functional theory method. It is found that a unique geometry is not able to accurately describe the whole adsorption isotherm. The use of slit-shaped pores gives overall better results, although the low-pressure regime is more accurate when cylindrical pores are used; reasons for this are discussed. The pore size distributions from the density functional theory are in reasonable agreement with the geometrical ones, giving the same shape and mean pore width and similar porosities in the four materials. Since it is known that the density functional theory gives excellent results for the adsorption isotherms (approximation b above), this comparison tests the independent pore model directly.

1. Introduction

Density functional theory (DFT) has proved to be a very useful tool for analyzing the adsorption behavior of porous materials and, in particular, in obtaining pore size distributions (PSDs).[1−4] DFT offers several advantages over other methods for PSD determination,[3−5] such as those based on the Kelvin equation and the semiempirical methods. In particular, DFT adsorption isotherms are in excellent agreement with molecular simulations,[1] and the method is not restricted to subcritical temperatures or to large pore widths, in contrast to Kelvin based methods. However, two important assumptions are made when DFT is used to model adsorption in an amorphous material: (a) that the material is made up of a collection of independent, noninterconnected pores of some simple, defined geometry (usually of slit or cylindrical shape) (we shall refer to this approximation as the *independent pore model*) and (b) that adsorption in these pores can be accurately described by DFT. Once the adsorption isotherm is obtained for a model glass, a PSD of the material can be inferred by fitting a linear combination of isotherms predicted from DFT to that obtained experimentally. To establish the accuracy of these methods is a difficult task, since there is no direct way to verify the PSD obtained. Moreover, it is not straightforward to distinguish errors due to the approximations made in modeling the individual pores from those due to the model used for the material as a whole.

Gelb and Gubbins[6] proposed a new approach to model porous silica glasses, using quench molecular dynamics (MD) methods that mimic the experimental processes in which these materials are produced. The resulting model glasses have a pore topology, porosity, surface area, and adsorption isotherm behavior similar to those of the real glasses. A major advantage of these model materials is that they are precisely characterized at the molecular level, and hence they provide an ideal framework in which to test different approaches used in practice to characterize amorphous systems, where various approximations and assumptions need to be made.

Controlled-pore glasses (CPGs) are widely used as a stationary phase in chromatography.[7,8] These materials

* Corresponding author. E-mail: lvega@icmab.es. Tel: + 34 93 580 18 53. Fax: + 34 93 580 57 29. Permanent address: Institut de Ciència de Materials de Barcelona (ICMAB-CSIC), Campus de la UAB, 08193 Bellaterra, Barcelona, Spain.

[†] Universitat Rovira i Virgili.

[‡] Washington University in St. Louis.

[§] North Carolina State University.

(1) Lastoskie, C.; Gubbins, K. E.; Quirke, N. *Langmuir* **1993**, *9*, 2693.

(2) Ravikovitch, P. I.; Vishnyakov, A.; Russo, R.; Neimark, A. V. *Langmuir* **2000**, *16*, 2311.

(3) Lastoskie, C. M.; Gubbins, K. E. In *Molecular Modeling and Theory in Chemical Engineering*; Chakraborty, A., Ed.; Advances in Chemical Engineering, Vol. 28; Academic Press: San Diego, 2001; p 203.

(4) Pikunic, J.; Lastoskie, C. M.; Gubbins, K. E. In *Handbook of Porous Solids*; Schüth, F., Sing, K. S. W., Weitkamp, J., Eds.; Wiley-VCH: Weinheim, 2002; Chapter 2.5.1, pp 182−236.

(5) Rouquerol, F.; Rouquerol, J.; Sing, K. *Adsorption by Powders & Porous Solids*; Academic Press: London, 1999.

(6) Gelb, L. D.; Gubbins, K. E. *Langmuir* **1998**, *14*, 2097.

(7) Haller, W. *Nature* **1965**, *206*, 693.

(8) Schnabel, R.; Langer, P. *J. Chromatogr.* **1991**, *544*, 137.

10.1021/la034686v CCC: $25.00
Published on Web 00/00/0000 PAGE EST: 12.9

have excellent mechanical properties and can be prepared with a wide range of porosities and pore sizes.[9] They can be modified to include a variety of functional groups, and the adsorption strength of the glasses can be adjusted over a wide range of values.[8] Although CPGs were developed for use in size exclusion chromatography, derivatized glasses can show a high chemical affinity for certain biomolecules and can even be used as catalytic agents and bioreactors.[7]

Gelb and Gubbins[10] obtained the nitrogen adsorption isotherms in these materials using Monte Carlo simulations. They also determined the geometrical PSD of the model porous glasses (the "real" or "exact" PSD) by using spherical probes. This PSD serves as the basis to test the accuracy of different methods used to obtain PSDs from other techniques. A study was carried out[10] on the validity of the Barrett−Joyner−Halenda (BJH) method to obtain the distribution of void volume in such model porous glasses. It was concluded that the PSDs obtained using the BJH method differ in a systematic way from those determined directly by geometrical means. The BJH method yields PSDs which are narrower and have most probable pore diameters about 10 Å smaller than the exactly known geometric PSDs. In a different work, Kanda et al.[11] applied a condensation model for cylindrical pores with a modified Kelvin equation, considering a meniscus curvature in a more realistic way. These authors, previously, developed and tested this model in nanopores with ideal geometry (cylindrical[12] and slit-shaped[13]), obtaining good agreement with simulations. To test their model versus a realistic geometry, they used "system A" from the work of Gelb and Gubbins[10] and compared the geometrical PSD versus the one obtained with the Kanda et al.[11] condensation model. The agreement obtained was very good. However, they could not determine the PSDs of the rest of the samples because the desorption branches and the range of the hysteresis they needed in their approach were not available.

In a series of articles, Monson and co-workers have performed a systematic study of adsorption in disordered porous materials, including porous glasses, by using different theoretical tools.[14−18] These materials were generated in both lattice and off-lattice systems, in a manner similar to that of Gelb and Gubbins.[6] They investigated the stability of the states associated with the adsorption/desorption isotherms, by grand canonical MD methods.[14] One of their interesting conclusions is that the grand canonical Monte Carlo (GCMC) hysteresis reflects experimental behavior more closely than has been previously appreciated. Of particular interest is their study of the interplay between hysteresis and equilibrium behavior associated with capillary condensation in a disordered matrix.[16,17] Their study indicates that for lattice models of xerogels and porous glasses the hysteresis behavior is not associated with a simple van der Waals metastability accompanying a first-order phase transition. Whether this applies to off-lattice versions of these systems still remains an open question. It is important to notice that they never made any assumption about the connectivity of the void space; neither did they invoke percolation concepts. This demonstrates the validity of a statistical mechanical theory of hysteresis in disordered porous media.

We use here a DFT approach based on the fundamental measure theory (FMT) in conjunction with a regularization method to characterize model porous glasses. The approach is applied to the CPG materials modeled by Gelb and Gubbins.[10] We have recently published[19] an exhaustive comparison between FMT and GCMC simulations for pores of simple geometry, establishing the accuracy of the theory for individual slitlike and cylindrical pores of these particular systems. Some authors have also studied the influence of having different geometries in the adsorption behavior of simple fluids. In particular, Reszko-Zygmunt et al.[20] investigated the phase behavior of LJ fluids in pores formed between two cylindrical walls, for a wide range of cylinder radius. Also, Goulding et al.[21] used the Rosenfeld FMT for mixtures in very narrow pores, obtaining the size selectivity in such narrow cylindrical pores and ion channels.

In this work, we test the DFT method by comparing PSDs obtained with this approach to the exact PSD for the model glasses of Gelb and Gubbins. Since we know that the DFT gives good results for adsorption in single pores,[19] such a comparison tests the hypothesis that the disordered material can be approximated as a collection of pores of some simple geometry, but having different pore widths. Additionally, we determine the most appropriate geometry to model porous glasses with this approach.

Apart from the ones mentioned above, an additional possible source of errors in obtaining PSDs is the fact that solving the adsorption integral equation, from which the PSD is inferred, is an "ill-posed" problem, that is, there are several PSD functions compatible with the experimental adsorption isotherm. Hence, additional insight on the problem is required to give an adequate, physically relevant solution. The inversion of the integral can be performed by proposing an analytical function, as a reasonable representation of the PSD, or by direct numerical inversion. The analytical functions are usually based on physical arguments, and their parameters are fitted to the adsorption data. However, as Davies et al.[22] pointed out, there is a danger in constraining the PSD to conform to the particular functional form adopted. The danger is that we are no longer determining whether *any* PSD can be fitted to the data, but rather whether a PSD conforming to the proposed functional form exists. In contrast, the numerical inversion of the integral shows the advantage of being more flexible, since the PSD is not constrained a priori to any functional form. An elegant and powerful way to solve this integral equation is by using regularization methods.[2,22,23] These methods also need additional information on the system, which is used to select one of the PSDs among all possible satisfying the

(9) Elmer, T. H. In *ASM Engineered Materials Handbook*; Schneider, S. J., Jr., Ed.; ASM: Materials Park, OH, 1991; Vol. 4, pp 427−432.
(10) Gelb, L. D.; Gubbins, K. E. *Langmuir* **1999**, *15*, 305.
(11) Kanda, H.; Miyahara, M.; Higashitani, K. *Langmuir* **2000**, *16*, 6064.
(12) Yoshioka, T.; Miyahara, M.; Okazaki, M. *J. Chem. Eng. Jpn.* **1997**, *30*, 274.
(13) Miyahara, M.; Kanda, H.; Yoshioka, T.; Okazaki, M. *Langmuir* **2000**, *16*, 4293.
(14) Sarkisov, L.; Monson, P. A. *Langmuir* **2000**, *16*, 9857.
(15) Sarkisov, L.; Monson, P. A. *Phys. Rev. E* **2000**, *61*, 7231.
(16) Kierlik, E.; Monson, P. A.; Rosinberg, M. L.; Sarkisov, L.; Tarjus, G. *Phys. Rev. Lett.* **2001**, *87*, 055701.
(17) Sarkisov, L.; Monson, P. A. *Phys. Rev. E* **2002**, *65*, 11202.
(18) Woo, H.-J.; Sarkisov, L.; Monson, P. A. *Langmuir* **2001**, *17*, 7475.
(19) Figueroa-Gerstenmaier, S.; Blas, F. J.; Bonet Avalos, J.; Vega, L. F. *J. Chem. Phys.* **2003**, *118*, 830.
(20) Reszko-Zygmunt, J.; Rzysko, W.; Sokolowski, S.; Sokolowska, Z. *Colloids Surf., A* **2002**, *208*, 199.
(21) Goulding, D.; Hansen, J.-P.; Melchionna, S. *Phys. Rev. Lett.* **2000**, *85*, 1132.
(22) Davies, G. M.; Seaton, N. A.; Vassiliadis, V. S. *Langmuir* **1999**, *15*, 8235.
(23) Gusev, V. Y.; O'Brien, J. A.; Seaton, N. A. *Langmuir* **1997**, *13*, 2815.

inversion equation from the knowledge of the experimental adsorption isotherms.[24]

Seaton et al.[25] first determined PSDs in porous carbons using a molecular model and nitrogen adsorption measurements. They used local DFT[26,27] to model nitrogen isotherms and fitted an analytical function to the experimental data. The same procedure has been successfully applied to other materials, such as microporous carbons[1] and activated carbon fiber.[28] Neimark et al.[29] obtained the PSD of MCM-41 adsorbents (cylindrical pores) by means of nitrogen and argon adsorption using nonlocal DFT (NLDFT). Other authors[2,25] have applied a similar procedure, with different adsorbates, to characterize microporous carbonaceous materials. Gusev and coworkers[23] and Davies and Seaton[30] have used GCMC simulations combined with regularization methods to obtain the PSD of activated carbons. MCM-41 and SBA-15 have also been recently characterized by Ravikovitch and Neimark using NLDFT.[31]

To check the validity of the DFT approach for obtaining reliable PSD of porous glasses, we use the model materials prepared by Gelb and Gubbins[10] as the "experimental" systems. The molecular parameters for the solid walls and the fluid inside them take the same values as in their work. In this sense, all deviations between predictions from the FMT calculations and the experimental data can be ascribed to limitations of the theoretical approach or to the model chosen for the material, that is, independent pores of a given geometry. We present and discuss results of theoretical adsorption isotherms of nitrogen obtained for cylindrical and slitlike pores, over a wide range of pore sizes. The PSDs are obtained in a systematic way. We first reconstruct the adsorption isotherm, using the set of theoretical isotherms obtained from FMT for pores of different sizes but weighted with the geometrical PSDs.[10] Both geometries, cylindrical and planar, are considered. In a second step, the PSDs are obtained from the inversion of adsorption integral equations for four materials when cylindrical and slitlike geometries are considered to model the material, along with a test that the method works well. Finally, we discuss the influence of the fluid−fluid and solid−fluid interaction parameters on the adsorption behavior.

2. Fundamental Measure Density Functional Theory

In the formulation of the DFT used here, we follow the work by Kierlik and Rosinberg.[32] When studying adsorption phenomena, it is convenient to work under constant chemical potential μ. Therefore, we focus our attention on the grand potential density functional of the system,

$$\Omega[\rho(\mathbf{r})] \equiv F\,[\rho(\mathbf{r})] - \int \mathrm{d}r\; \rho(\mathbf{r})[\mu - \phi_{\mathrm{ext}}(\mathbf{r})] \qquad (1)$$

where the first term on the right-hand side is the intrinsic Helmholtz free energy functional, and in the second term the expression $\phi_{\mathrm{ext}}(\mathbf{r})$ takes into account the potential field imposed by the wall. In this expression, $\rho(\mathbf{r})$ is the particle number density.

In the FMT formulation, the grand potential takes the form

$$\Omega[\rho(\mathbf{r})] = k_{\mathrm{B}}T \int \mathrm{d}\mathbf{r}\rho(\mathbf{r})[\ln(\Lambda^3\rho(\mathbf{r})) - 1] + k_{\mathrm{B}}T \int \mathrm{d}\mathbf{r}\Phi(\{\bar{n}_\alpha(\mathbf{r})\}) + \frac{1}{2}\int \mathrm{d}\mathbf{r} \int \mathrm{d}\mathbf{r}'\rho(\mathbf{r})\rho(\mathbf{r}')\phi_{\mathrm{att}}(|\mathbf{r} - \mathbf{r}'|) - \int \mathrm{d}\mathbf{r}\rho(\mathbf{r})[\mu - \phi_{\mathrm{ext}}(\mathbf{r})] \qquad (2)$$

In this expression, the first term is the ideal gas contribution to the free energy. The second term is the excess free energy of the hard-sphere reference system in a weighted density approximation.[32] The third term describes the effect of the attractive interactions between particles, ϕ_{att}, introduced in a mean-field approximation. The last term represents the contribution of the bulk chemical potential as well as the effects of the walls of the pore, introduced through the external field $\phi_{\mathrm{ext}}(\mathbf{r})$. Λ is the de Broglie wavelength, k_{B} is Boltzmann's constant, and T is the absolute temperature.

According to Kierlik and Rosinberg,[32] the excess free energy density of the reference system of hard spheres, $k_{\mathrm{B}}T\Phi(\{\bar{n}_\alpha(\mathbf{r})\})$, is assumed to be a function of the weighted densities, the latter defined as

$$\bar{n}_\alpha(\mathbf{r}) = \int \mathrm{d}\mathbf{r}'\omega^{(\alpha)}(\mathbf{r} - \mathbf{r}')\rho(\mathbf{r}') \qquad (3)$$

with $\alpha = 0$, 1, 2, and 3. The four weight functions $\omega^{(\alpha)}(r)$ are related to the Heaviside step function, $\Theta(r)$, and its derivatives. These weight functions are independent of the density, and their expression can be found in ref 32. The hard-sphere excess free energy contribution has the form[32]

$$\Phi(\{\bar{n}_\alpha\}) = -\,\bar{n}_0 \ln(1 - \bar{n}_3) + \frac{\bar{n}_1\bar{n}_2}{1 - \bar{n}_3} + \frac{1}{24\pi}\frac{\bar{n}_2{}^3}{(1 - \bar{n}_3)^2} \qquad (4)$$

The equilibrium properties of the fluid can be obtained by minimizing the grand potential functional, eq 2, with respect to the local density, at constant chemical potential, μ, and under appropriate boundary conditions. The above requirements result in the Euler−Lagrange equation

$$\mu = k_{\mathrm{B}}T \ln(\Lambda^3\rho(\mathbf{r}'')) + \int \mathrm{d}\mathbf{r} \sum_\alpha \omega^{(\alpha)}(|\mathbf{r} - \mathbf{r}''|)\frac{\partial\Phi}{\partial\bar{n}_\alpha(\mathbf{r})} + \int \mathrm{d}\mathbf{r}\rho(\mathbf{r})\phi_{\mathrm{att}}(|\mathbf{r} - \mathbf{r}'|) + \phi_{\mathrm{ext}}(\mathbf{r}'') \qquad (5)$$

which is an implicit relationship to be satisfied at every space point $\mathbf{r}''$. The functional inversion of eq 5 yields the density profile in terms of the chemical potential, the attractive and external potential fields, and the geometry of the particles. Details on the inversion of this equation in the case of a fluid adsorbing onto cylindrical walls of diameter H, unbounded in the axial direction, were given in our previous work.[19]

3. Molecular Model

Since our first goal is to check the validity of the independent pore model for the CPGs of Gelb and Gubbins,

(24) Press, W. A.; Teukolsky, S. A.; Vetterling, W. T.; Flannery, B. P. *Numerical Recipes in Fortran*, 2nd ed.; Cambridge University Press: New York, 1992.
(25) Seaton, N. A.; Walton, J. P. R. B.; Quirke, N. *Carbon* **1989**, *27*, 853.
(26) Evans, R.; Tarazona, P. *Phys. Rev. Lett.* **1984**, *52*, 557.
(27) Evans, R.; Marini Bettolo Marconi, U.; Tarazona, P. *J. Chem. Phys.* **1986**, *84*, 2376. Evans, R.; Marini Bettolo Marconi, U.; Tarazona, P. *J. Chem. Soc., Faraday Trans. 2* **1986**, *82*, 1763.
(28) El-Merraoui, M.; Aoshima, M.; Kaneko, K. *Langmuir* **2000**, *16*, 4300.
(29) Neimark, A. V.; Ravikovitch, P. I.; Grün, M.; Schüth, F.; Unger, K. K. *J. Colloid Interface Sci.* **1998**, *207*, 159.
(30) Davies, G. M.; Seaton, N. A. *AIChE J.* **2000**, *46*, 1753.
(31) Ravikovitch, P. I.; Neimark, A. V. *Colloids Surf., A* **2001**, *187*, 11.
(32) Kierlik, E.; Rosinberg, M. L. *Phys. Rev. A* **1990**, *42*, 3382.

the molecular parameters used are the same as in the simulation of nitrogen adsorption on their model porous glasses of silica. The adsorption took place at standard conditions for nitrogen at the normal boiling temperature of 77 K.[6,10]

3.1. Fluid/Fluid Interactions. The nitrogen molecule is modeled as a spherical Lennard-Jones (LJ) particle, with a "cut-and-shifted potential", $\phi^{LJ}(r)$. The LJ parameters ϵ/k_B (K) = 95.2 and σ (Å) = 3.75 were those used by Gelb and Gubbins.[6] In addition, all the LJ interactions were truncated at a cutoff radius $r_c = 2.52\sigma$.

We divide the potential into repulsive (reference) and attractive (perturbative) components, following the conventional Weeks, Chandler, and Andersen (WCA) perturbation scheme,[33] splitting the potential at the minimum, with $r_{min} = 2^{1/6}\sigma$. In this approach, the reference system is replaced by a system of hard spheres with a temperature-dependent diameter $d(T^*)$. We have used the mapping from LJ to hard spheres developed by Verlet and Weis[34] and Lu et al.,[35] with the coefficients $\eta_1 = 0.3837$, $\eta_2 = 1.035$, $\eta_3 = 0.4249$, and $\eta_4 = 1$, fitted by Peterson et al.[36] to match the bulk phase diagram of the LJ fluid.

The excess Helmholtz free energy per particle of the hard-sphere reference system, Φ, given in eq 4, corresponds to the scaled particle theory (SPT)[37,38] or, equivalently, the Percus−Yevick (PY) equation of state[39−41] if the system is homogeneous, $\rho(\mathbf{r}) \equiv \rho$. Moreover, the weighted densities defined in eq 3 coincide with the variables of the SPT[37,38] in this limit and can be written in terms of the so-called fundamental measures characterizing the particle ($\bar{n}_0 = \rho$, $\bar{n}_1 = R\rho$, $\bar{n}_2 = 4\pi R^2\rho$, $\bar{n}_3 = (4/3)\pi R^3\rho$).

3.2. Solid−Fluid Interactions. Gelb and Gubbins[6] proposed a protocol for the preparation of molecular models of porous glass by quench molecular dynamics simulations: a binary mixture of molecules is placed in a box and equilibrated at a given temperature at supercritical conditions; then, the system is quenched at constant density to a subcritical state point within the spinodal curve. The mixture starts to phase separate into a phase made of winding and connected segments of roughly cylindrical geometry (the "boron oxide rich phase") and a second liquid phase (the "silica-rich phase"). The simulation continues until the desired pore size is obtained. In a third step, the system is quenched further, allowing the surface structure to form and the material to solidify. Finally, after annealing, the "2"-rich phase is removed from the system, leaving a material with the desired porosity and similar in structure to the real material. Following this general procedure, Gelb and Gubbins generated the model porous glasses to which we will refer in our analysis. Four samples in particular were characterized[10] using GCMC and geometrical probes. The materials have average pore sizes of approximately 3.3, 3.9, 4.5, and 5.0 nm, respectively; all have porosities near 30%. In these models, the pores are fully connected, the void space being a single volume of very complex geometry, rather than several disconnected volumes.

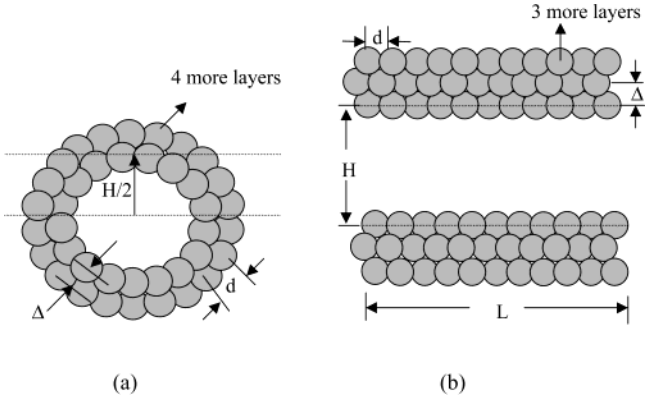

Figure 1. Structure of (a) cylindrical and (b) slitlike pores.

The LJ parameters for the substrate atoms in our work are those used in the previous work,[6,10] $\epsilon_{ss}/k_B = 230$ K and $\sigma_{ss} = 2.7$ Å. These parameters represent bridging oxygen atoms in silica, since previous simulations of adsorption on silica gels show that the omission of the silicon atoms is an acceptable approximation.[42] We use the Lorentz−Berthelot combining rules to model the LJ solid−fluid interactions.

For the DFT calculations, we use a crude model of these materials. We have considered two pore geometries, cylindrical and slitlike. In the first case, each pore is represented as an infinite cylinder where the wall atoms are single spherical LJ sites. These LJ spheres are laid out in six concentric layers separated by a distance Δ (=0.30 nm). Each layer is arranged in such a way that the atoms in the consecutive one are displaced $d/2$ ($d = 0.277$ nm) in both the angular and axial directions. The distance between adjacent atoms in the same layer is d. The resulting overall configuration of each layer can be described as a hexagonal lattice. These parameter values were chosen so that the total density of oxygen atoms in the CPG model of Gelb and Gubbins, 44.1 atoms/nm^2, and a material porosity of 30% are approximately reproduced.[10] The pore diameter H is defined as the distance between the centers of the particles on opposite sides of the innermost layer. Such a model is shown in Figure 1a. In the case of slitlike pores, the material is modeled by applying the same principles to a planar geometry, where the parameter H represents the distance between two identical parallel walls. In Figure 1b, a representation of such a pore can be found.

The total potential energy between a fluid molecule probe and the wall is calculated as the sum of its interactions with all the substrate atoms. For simplicity in the DFT calculations, we have considered an averaged potential, constructed from the previous one by integrating with respect to the angular and axial directions, preserving only the radial functional dependence. For slitlike pores, the potential is averaged over translations parallel to the walls. In this sense, the pores are modeled as unstructured.

3.3. Pore Properties. The mean pore fluid density, $\langle\rho\rangle$, is defined by

$$\langle\rho\rangle = \frac{\int d\mathbf{r}\rho(\mathbf{r})}{\int d\mathbf{r}} \qquad (6)$$

(33) Weeks, J. D.; Chandler, D.; Andersen, H. C. *J. Chem. Phys.* **1971**, *54*, 5237.
(34) Verlet, L.; Weis, J. J. *Phys. Rev. A* **1972**, *5*, 939.
(35) Lu, B. Q.; Evans, R.; Telo da Gama, M. M. *Mol. Phys.* **1985**, *55*, 1319.
(36) Peterson, B. K.; Walton, J. P. R. B.; Gubbins, K. E. *J. Chem. Soc., Faraday Trans. 2* **1986**, *82*, 1789.
(37) Reiss, H.; Frisch, H. L.; Lebowitz, J. L. *J. Chem. Phys.* **1959**, *31*, 369.
(38) Helfand, E.; Frisch, H. L.; Lebowitz, J. L. *J. Chem. Phys.* **1961**, *34*, 1037.
(39) Wertheim, M. S. *Phys. Rev. Lett.* **1963**, *10*, 321.
(40) Thiele, E. J. *Chem. Phys.* **1963**, *39*, 474.
(41) Lebowitz, J. L. *Phys. Rev.* **1964**, *133*, A895.
(42) Brodka, A.; Zerda, T. W. *J. Chem. Phys.* **1991**, *85*, 3710. MacElroy, J. M. D. *Langmuir* **1993**, *9*, 2682.

where the integrals are taken over the volume of the pore. The excess density is defined as the deviation of the average density with respect to the bulk values, that is,

$$\langle \rho^{E} \rangle \equiv \langle \rho \rangle - \rho_{bulk} \tag{7}$$

There is a difference in the way we calculate the nitrogen average density inside the pore here and in our previous work.[19] Since Gelb and Gubbins used the Connolly surface definition of the pore volume, we have employed the same definition and have taken $H - \sigma_{ss}$ as the pore diameter. Following this definition, for cylindrical pores we have

$$\langle \rho^{E} \rangle = \frac{8}{(H - \sigma_{ss})^2} \int_0^{(H-\sigma_{ss})/2} (\rho(r) - \rho_{bulk}) r \, dr \tag{8}$$

while for slitlike pores, the excess density inside the pore is given by

$$\langle \rho^{E} \rangle = \frac{1}{(H - \sigma_{ss})} \int_0^{H-\sigma_{ss}} (\rho(z) - \rho_{bulk}) \, dz \tag{9}$$

Finally, it is important to note that the experimental adsorption isotherm represents the amount of fluid adsorbed per unit of volume of the material, while the theoretical adsorption isotherm is the fluid adsorbed per unit of void volume. Therefore, it is necessary to use the porosity of the material to relate these different concepts of volume.

4. Pore Size Distribution Calculations

The calculation of the PSD of materials from adsorption data is a problem which has been addressed by several authors (see, for instance, the work by Ravikovitch et al.,[2] Davies et al.,[22] and Davies and Seaton[30]). In the model of independent pores, the adsorbance is related to the PSD by the expression

$$\Gamma_V(\mu^*) = \mathscr{P} \int_{H_{min}}^{H_{max}} \rho^{E}(\mu^*, H) f(H) \, dH \tag{10}$$

where $\Gamma_V(\mu^*)$ represents the adsorbate particle number per unit volume of adsorbent material (in Å^{-3}) at reduced chemical potential $\mu^* = \mu/\epsilon$; $\rho^{E}(\mu^*, H)$, the kernel function, gives the contribution to the adsorption isotherm of an ideally homoporous material characterized by the pore width (or diameter) H, in units of excess particle number per void volume of the pore (in Å^{-3}), and $f(H)$ is the desired PSD. The size H is also given in Å, while $f(H)$ is given in Å^{-1}. Finally, $\mathscr{P}$ is the porosity (void volume per total volume).

Equation 10 is an "inhomogeneous Fredholm equation of the first kind",

$$g(x) = \int_a^b k(x,s) u(s) \, ds \tag{11}$$

and its solution $u(x)$ is unique only under very restrictive conditions.[24] If the kernel $k(x,s)$ is not invertible, one faces an ill-posed problem.

To obtain a numerical estimate of $f(H)$, eq 10 can be written as a summation:

$$\Gamma_V(\mu^*) = \mathscr{P} \sum_i \rho^{E}(\mu^*, H_i) f(H_i) \Delta H_i \tag{12}$$

where $\Gamma_V(\mu^*)$ is the experimental adsorption isotherm given as a sequence of values of the adsorbance at discrete values of the chemical potential, μ_j^*, $\rho^{E}(\mu_j^*, H_i)$ is a matrix

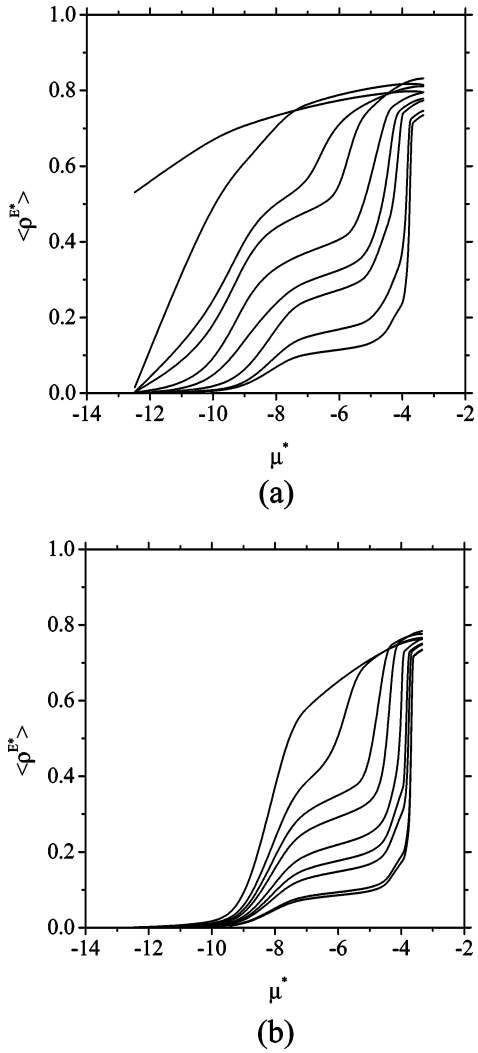

Figure 2. Adsorption isotherms of nitrogen at 77 K for (a) cylindrical pores of diameters H = 3.2, 4.0, 4.8, 5.6, 7.2, 8.8, 10.4, 16.0, and 17.6σ and (b) slitlike pores of diameters H = 1.6, 2.4, 3.2, 4.0, 4.8, 5.6, 7.2, 8.8, 10.4, 16.0, and 17.6σ, starting from left to right.

of theoretical isotherms, each row calculated at values of H_i at fixed chemical potential μ_j^*, and $f(H_i)$ is the solution vector whose components represent an estimate of the desired PSD. Therefore, $f(H_i)\Delta H_i$ is the fraction of void volume of pores, in the interval of pore sizes ΔH_i with respect to the total void volume. Equation 12 can only be inverted, aiming at the determination of the vector $f(H_i)$, if the matrix $\rho^{E}(\mu_j^*, H_i)$ is square and its determinant is nonzero. In general, if this determinant is small, the solution is very sensitive to small deviations between the theoretical and experimental adsorbances.

In our case, the matrix $\rho^{E}(\mu_j^*, H_i)$ is not square and therefore eq 12 cannot be directly inverted. Hence, a simple regularization procedure has been introduced. Regularization is based on the consideration of additional information on the system, which can be introduced to brake the uncertainty in the solution, and limits the sensitivity to small errors. Here, we can make use of the fact that $f(H_i)$ should be non-negative. A second condition is to require that for any real sample, the pore size distribution must be a rather smooth function of its argument H. As a measure of the smoothness, we use the size of the second derivative of $f(H_i)$. Then, one replaces the direct inversion of eq 12 by a variational problem in which one has to minimize a function, which takes into account the distance

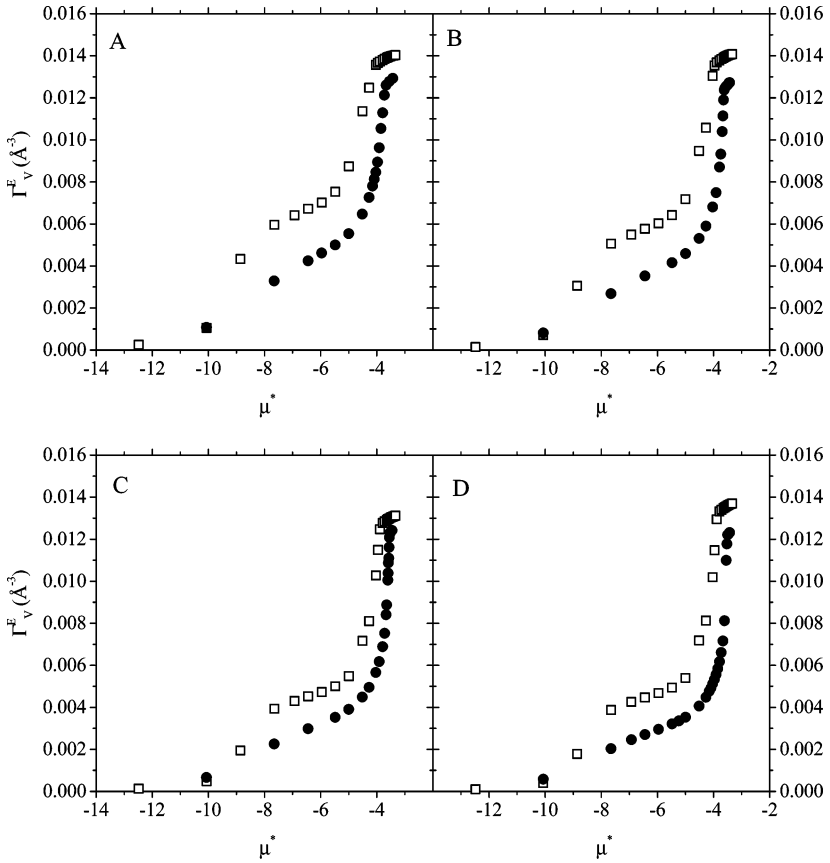

Figure 3. Adsorption isotherms reconstructed using theoretical isotherms of cylindrical pores obtained with FMT calculations and weighted with the geometrical PSDs (squares). These are compared with the experimental adsorption isotherms (ref 10) (circles) for the four different materials, A, B, C, and D (indicated by the corresponding labels).

of the experimental and theoretical isotherms, as well as the smoothness of the solution. We have chosen the function

$$F = \sum_j^n (\Gamma_V(\mu_j^*) - \mathscr{P}\sum_i^m \rho^E(H_i,\mu_j^*) f(H_i)\Delta H_i)^2 + \gamma_R{}^2 \sum_i^m \left(\frac{d^2 f(H_i)}{dH_i{}^2}\right)^2 \Delta H_i{}^2 \quad (13)$$

The problem[43] is now reduced to finding the $f(H_i)$ such that the first term of the previous equation is small (a good fit to the data) and the second one is small too (a smooth PSD), with $f(H_i) \geq 0$ (no negative pore area). The regularization parameter γ_R has to be conveniently chosen to give an adjustment to the relative weight, or importance, of the two terms. If the model is good and the data are very accurate, γ_R should be very small. Large values of γ_R will increase the smoothness of the resulting curve but will then favor deviations between the theoretical and experimental isotherms.

Finding the vector $f(H_i)$ that minimizes F subject to the constraint that $f(H_i) \geq 0$ is a standard problem in pure linear algebra. Here we have employed the Levenberg−Marquart (LM) method.[24] The second derivative on the right-hand side of eq 13 was evaluated by finite increments. We also used the following boundary conditions: $f(H_1) = 0$ when $H_1 = 0$, and $f(H_n) = 0$. A functional convergence tolerance of 1×10^{-14} has been used for all calculations done here. An additional problem is the fact that the function F presents several minima. To find the absolute minimum of F and, therefore, the suitable solution of the inversion problem, we have developed a Monte Carlo program to generate different initial guesses for $f(H_i)$. When the LM algorithm finds a solution of the minimum squared difference, the solution is kept, and the algorithm is run again. The new solution is also kept and compared to the previous one. The program will keep only the smaller between these two, for comparison with the next solution, in which the small one will be kept again. We follow this procedure 100 times, observing no further improvement.

5. Results and Discussion

Taking advantage of the fact that we are using molecular models, where we can systematically study the influence of different parameters on a particular property, we will proceed in the following way. First, we calculate the adsorption isotherms of individual pores (for both cylindrical and slitlike geometries) by means of FMT; the accuracy of the theory for these geometries and model in a wide range of pore sizes was proved already in our previous work.[19] Second, we use the geometrical PSD measured in ref 10 to weight the individual isotherms, thus reconstructing the overall isotherm. In this way, we check the accuracy of the individual pore model as an appropriate representation of real porous glasses. Third, we estimate the PSD of the material by inversion of the adsorption integral using the regularization method described above and considering the two pore geometries. The effect of considering additional pore sizes in the analysis is also investigated for the case of slitlike pores.

(43) Jaroniec, M.; Kruk, M.; Olivier, J. P.; Koch, S. In *Characterisation of Porous Solids V*; Unger, K. K., Kreysa, G., Baselt, J. P., Eds.; Studies in Surface Science and Catalysis, Vol. 128; Elsevier Science B.V.: Amsterdam, 2000; pp 71−80.

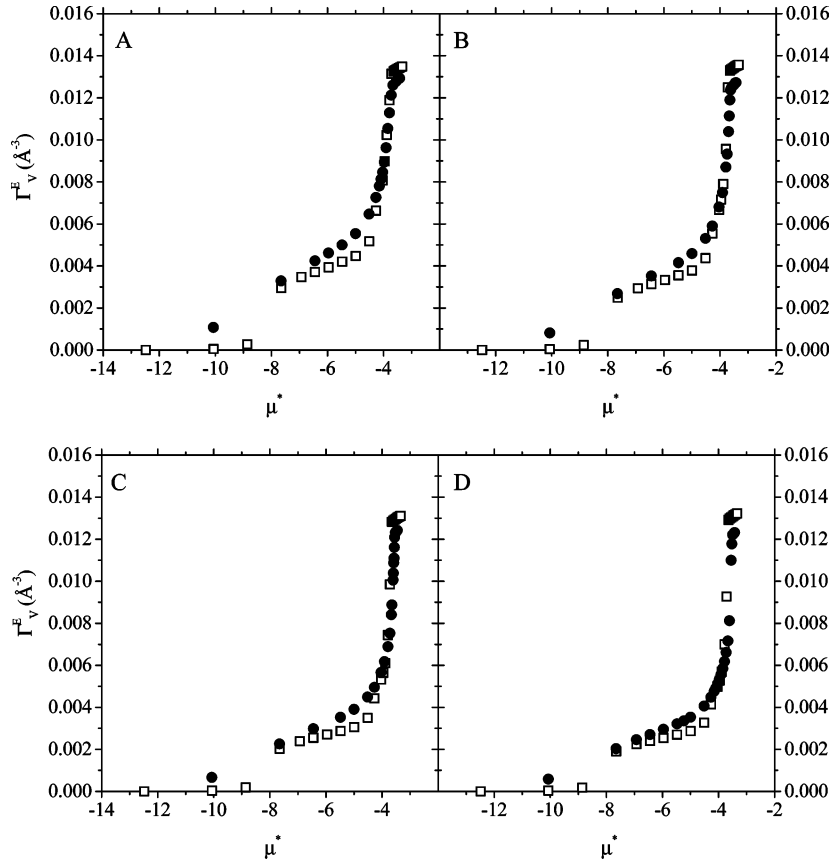

Figure 4. Adsorption isotherms reconstructed using theoretical isotherms of slitlike pores obtained with FMT calculations and weighted with the geometrical PSDs (squares). These are compared with the experimental adsorption isotherms (ref 10) (circles) for the four different materials, A, B, C, and D.

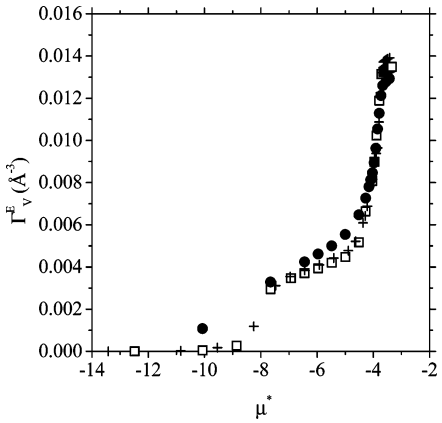

Figure 5. Adsorption isotherms reconstructed using theoretical isotherms of slitlike pores obtained with FMT, weighted with the geometrical PSDs. Two different sets of molecular parameters are used: original parameters from Gelb and Gubbins (refs 6 and 10) (squares) and those from Table 1 (crosses). The experimental adsorption isotherm (ref 10) (circles) for material A is shown.

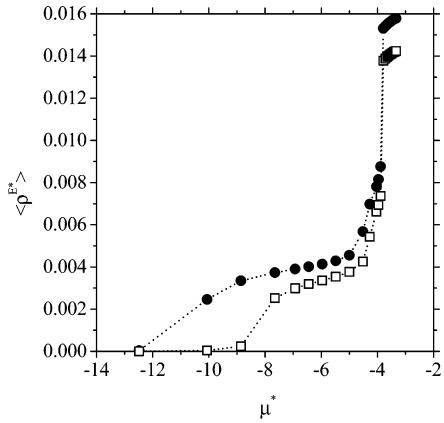

Figure 6. Adsorption isotherms of nitrogen at 77 K on a slitlike pore of $H = 33$ Å calculated with $\epsilon_{sf}^* = 2.0$ (circles) and with $\epsilon_{sf}^* = 1.55$ (squares).

To calculate the PSD of the material, a series of individual adsorption isotherms for both geometries were calculated. For slitlike pores, the distance between walls ranged from 6 to 66 Å, with intervals of 3 Å. In the case of cylindrical pores, the pore diameter used in the calculations ranged from 12 to 66 Å. In panels a and b of Figure 2, we present the collection of adsorption isotherms calculated for cylindrical and slitlike pores, respectively. For clarity we show only selected sizes, in the range of diameters mentioned above. In general, in the cylindrical pores the adsorption occurs at lower pressures than in the homologous slitlike pores, and the total capacity is higher in the slitlike case. In the context of this work, it is relevant to compare the adsorption in narrow pores, where the pore geometry plays an essential role: notice,

Table 1. Values of the Pressure, $P^* = P\sigma^3/\epsilon$, and Density, $\rho^* = \rho\sigma^3/\epsilon$, of the Saturated Liquid Nitrogen in Reduced Units and the Molecular Interaction Parameters Fitted with the SPT Equation of State

saturation pressure	0.01477
density of saturated liquid	0.726

parameter	fluid−fluid	solid−fluid
σ (Å)	3.64	3.17
ϵ/k_B (K)	88.90	142.99

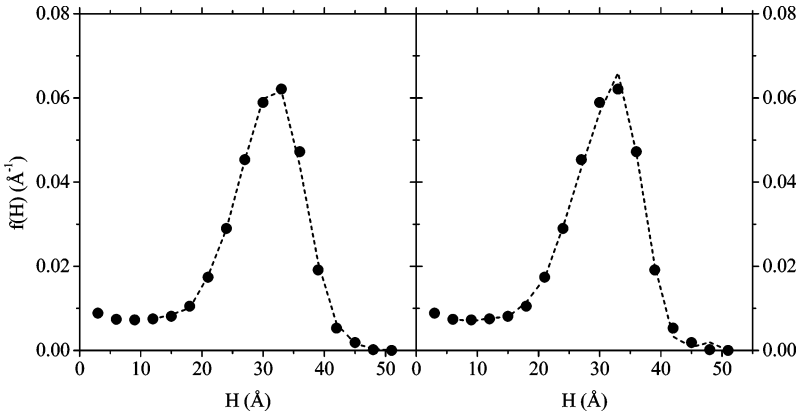

Figure 7. PSDs (dashed lines) obtained from the inversion of eq 13 using the theoretical isotherms for (a) the set of isotherms on cylinders from Figure 2a and (b) the set of isotherms on slitlike pores from Figure 2b. The symbols correspond to the geometrical distribution from the work of Gelb and Gubbins (ref 10) for sample A.

Table 2. Parameters and Results from the Fitting of Figure 7[a]

system	number of theoretical isotherms employed	number of points of the experimental isotherm	number of interpolated points of the experimental isotherm	γ_R	% $\mathscr{P}$	% deviation between isotherms[b]
A with cylinders	14	23	23	0.00001	28.0	0.020
A with slitlike pores	16	23	23	0.000001	29.0	0.018

[a] γ_R is the regularization parameter. [b] The deviation is defined as

$$\sum_j^n \frac{|\Gamma_V(\mu_j^*) - \mathscr{P}\sum_i^m \rho^E(H_i,\mu_j^*)f(H_i)\Delta H_i|}{\Gamma_V(\mu_j^*)} \times 100 \text{ (see eq 13).}$$

for instance, that the adsorption in a cylindrical pore of 12 Å (3.2σ) is equivalent to the adsorption in a planar pore of 6 Å (1.6σ). This will turn out to be important when calculating the PSD of adsorbent materials. A detailed discussion on the adsorption behavior depending on pore size and geometry was already presented in our previous work.[19]

5.1. Adsorption Isotherm Reconstruction. As a first step in validating our method, we use the individual adsorption isotherms obtained by FMT, weighted by the geometric PSD, according to eq 10, to predict the experimental adsorption isotherm of the four samples obtained by Gelb and Gubbins. We use the same range of pore diameters (12−66 Å) in both cases. A comparison between the predicted and the real isotherm tests the assumption that the material is made up of individual cylinders (or slitlike pores), assuming the same PSD but ignoring the interconnectivity of the real material.

The results for the cylindrical pore geometry are shown in Figure 3. As can be inferred from the figure, the reconstructed adsorption isotherm has the same shape as the experimental one, although the predicted adsorption is always higher, except for very low pressures, for the four materials considered. This discrepancy may have different causes: (a) the model used to represent the individual isotherms and the method to obtain them may not be appropriate; (b) the properties of the substrates may not be the same in both cases; (c) the equation of state for the bulk may not be accurate enough; (d) we began the FMT calculations at pore diameters of 12 Å, ignoring smaller pores; (e) the material is not well represented by a collection of individual cylinders.

Each of these points opens new possibilities; for instance, point e may suggest that either the cylindrical geometry is not well chosen or that the interconnectivity among the pores is more important than is usually assumed in modeling adsorbent materials. We first investigate point e by choosing a different pore geometry and proceeding in the same manner, before further investigating the rest of the points presented here.

In Figure 4, we show results equivalent to those of Figure 3, but using a linear combination of the individual isotherms of slitlike pores, according to eq 10. It is clear that in this case the overall agreement between the reconstructed isotherms and the experimental ones improves in all four cases considered, showing that CPGs are better represented by a collection of individual slitlike pores rather than cylindrical pores. However, there are some discrepancies at low pressures (low chemical potentials); the adsorption predicted by the planar geometry is much lower than the experimental one, while this region was described well by the cylindrical geometry (see Figure 3). At intermediate pressures, the adsorption in planar pores is still lower, with the inflection of the curve more pronounced than the experimental one. Finally, at high pressures, where capillary condensation occurs in the wider pores while the smaller ones are filled, the material, modeled as a collection of planar pores, slightly overpredicts the adsorption. This behavior is common to the four materials used.

There are two more points that require further investigation before proceeding to the inversion of the integral: the importance of the models used for the fluid and for the substrate. We first check the fact that the bulk fluids in DFT and simulations do not follow the same equation of state. To check this, we have taken the vapor−liquid equilibrium point of the phase diagram of nitrogen at the conditions reproduced by Gelb and Gubbins parameters[10] and fitted σ and ϵ using the SPT equation of state. In general, slightly different values of the parameters are expected, since we use different equations of state for the bulk for the same fluid. Besides, the use of a short cutoff

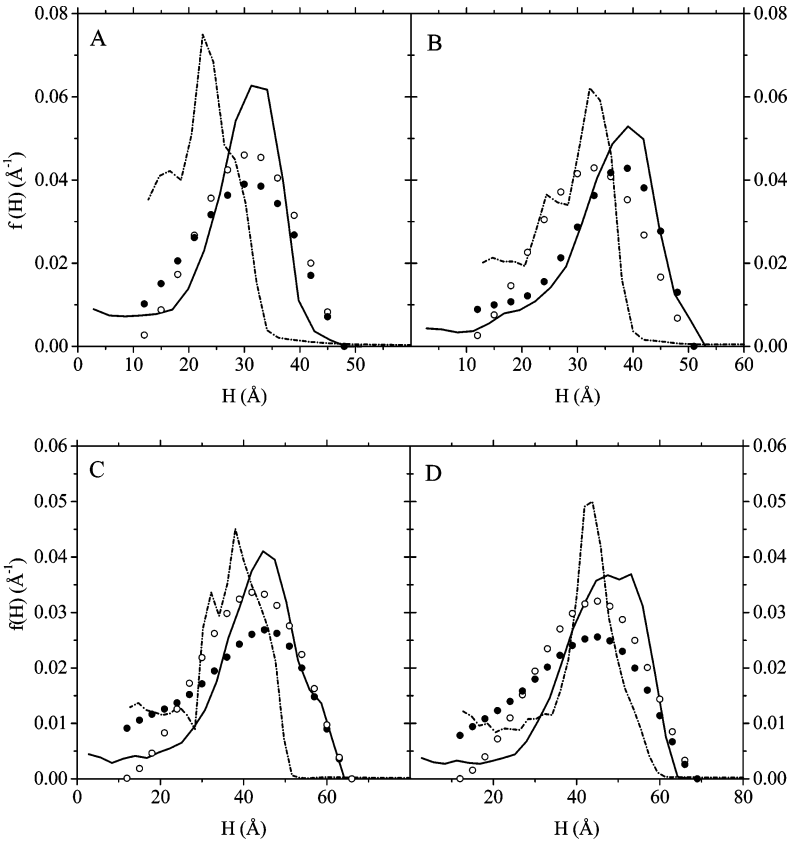

Figure 8. PSDs obtained in this work using cylindrical pores (open circles) and slitlike pores (filled circles), compared with geometrical PSDs (solid lines) and with BJH PSDs (dashed−dotted lines), both from ref 10 for each of the four systems A, B, C, and D.

Table 3. Parameters and Results from the Fitting of Figures 8 and 9 Using Cylindrical Pores[a]

system	number of theoretical isotherms employed	number of points of the experimental isotherm	number of interpolated points of the experimental isotherm	γ_R	$\%\mathscr{P}$	% deviation between isotherms[b]
A	13	19	21	30	21.6	21.51
B	14	20	21	50	19.5	27.31
C	19	22	20	70	18.3	19.90
D	20	26	21	110	17.7	22.73

[a] γ_R is the regularization parameter. [b] Deviations defined as in Table 2.

Table 4. Parameters and Results from the Fitting of Figures 8 and 10 Using Slitlike Pores[a]

system	number of theoretical isotherms employed	number of points of the experimental isotherm	number of interpolated points of the experimental isotherm	γ_R	$\%\mathscr{P}$	% deviation between isotherms[b]
A	13	19	21	1	26.7	15.58
B	14	20	21	1	25.5	17.32
C	19	22	20	10	22.5	19.43
D	20	26	21	30	23.1	20.59

[a] γ_R is the regularization parameter. [b] Deviations defined as in Table 2.

can make these differences bigger. Results are presented in Table 1. In Figure 5, we analyze the effect of using these new fluid−fluid parameters in calculating the set of isotherms inside the pores and their application to material A. As might be expected, no significant changes are observed at low pressures, where the adsorption is dominated by the solid−fluid interactions. Changes are visible at high pressures, where the fluid−fluid interaction is dominant, giving a higher adsorption than that obtained for the experimental material. From the individual analysis of each pore (not shown here), we see that the use of different fluid−fluid parameters is more important for the case of the small pores, while it becomes less relevant as the pore size is increased.

To determine the influence of the solid−fluid energy interaction parameter, we have performed a comparison of adsorption isotherms for two different values of ϵ_{sf}, keeping constant ϵ_{ss} and ϵ_{ff}. In Figure 6, we present the individual adsorption isotherm of a planar pore of $H = 33$ Å for $\epsilon^*_{sf} = 1.55$ (the value used in all the calculations presented here) and a more attractive wall, $\epsilon^*_{sf} = 2.0$. As expected, the adsorption is much stronger at low pressures in the second case, since the solid−fluid interactions are dominant in this region, and it is slightly higher in the rest of the isotherm. Note that the capillary condensation occurs in both cases at the same pressure, a consequence of keeping the same fluid−fluid interaction parameters.

Finally, we want to point out one more reason for possible deviations between the predicted and experimental adsorption isotherms. Although we have used in our model the same set of parameters described in ref 10 for the solid−fluid interaction, it is important to notice

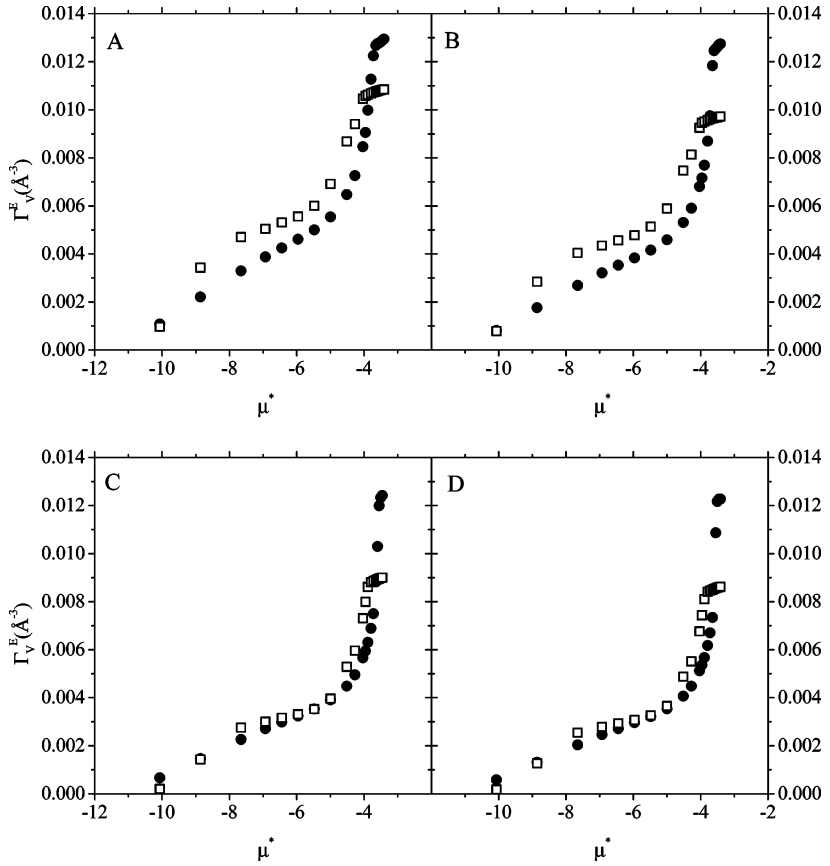

Figure 9. Adsorption isotherms obtained (squares) in this work using cylindrical pores to solve eq 13, compared with experimental isotherms (circles) from ref 10 for each of the four systems A, B, C, and D.

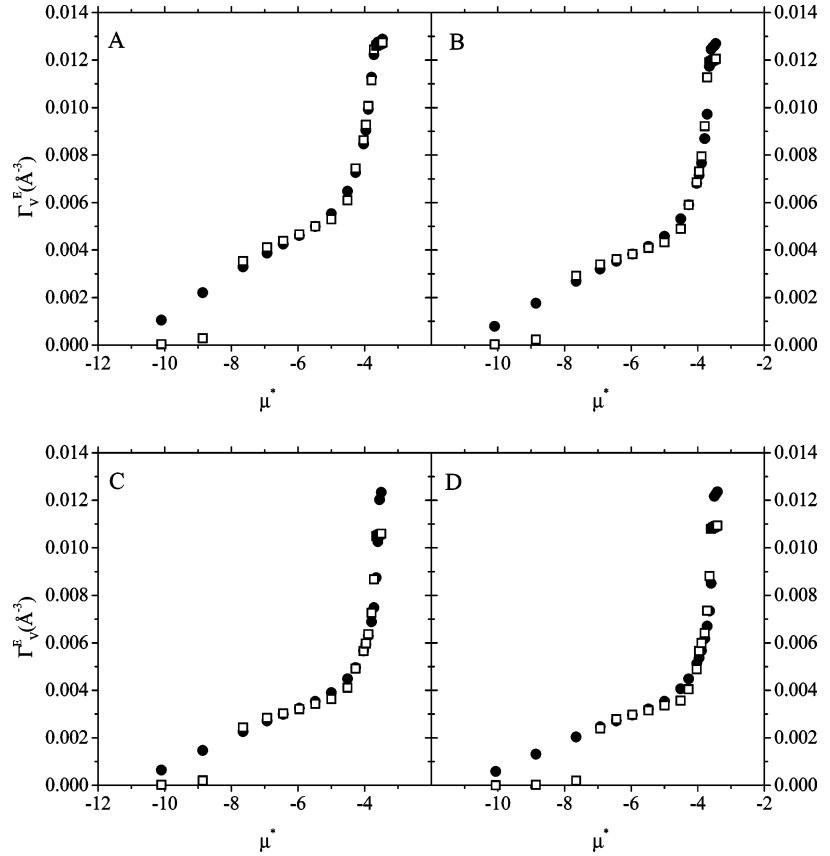

Figure 10. Adsorption isotherms obtained (squares) in this work using slitlike pores to solve eq 13, compared with experimental isotherms (circles) from ref 10 for each of the four systems A, B, C, and D.

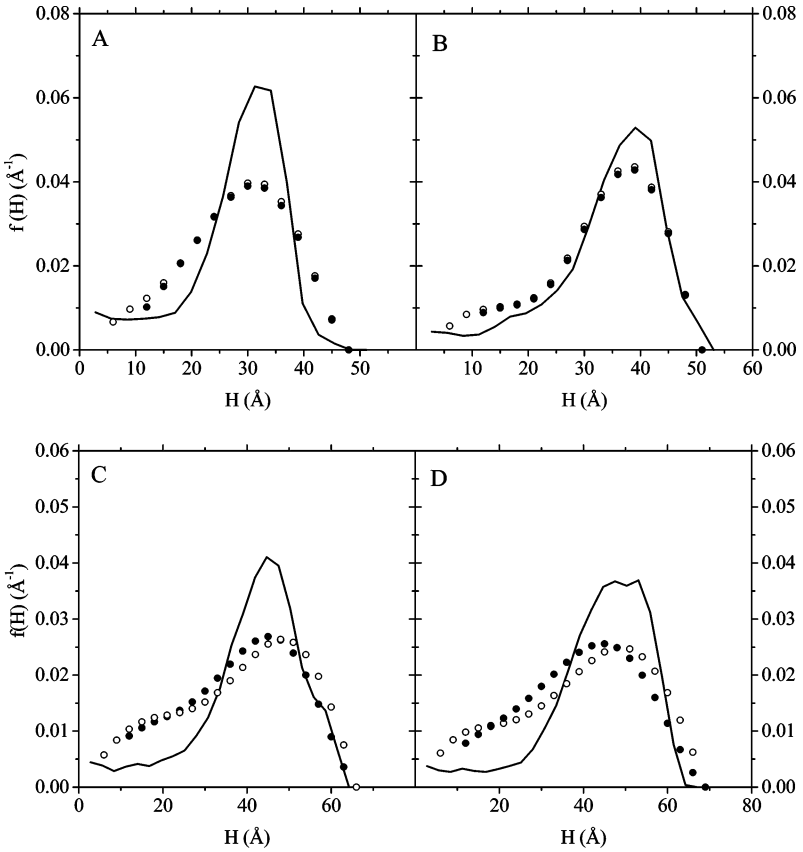

Figure 11. PSDs obtained in this work using slitlike pores (open circles), including narrower sizes and the previous PSD from Figure 8 (filled circles in Figure 8), compared with geometrical PSDs (solid lines in Figure 8) from ref 10 for each of the four systems A, B, C, and D.

Table 5. Parameters and Results from the Fitting of Figures 11 and 12 Using Slitlike Pores[a]

system	number of theoretical isotherms employed	number of points of the experimental isotherm	number of interpolated points of the experimental isotherm	γ_R	$\%\mathscr{P}$	% deviation between isotherms[b]
A	15	19	21	1	26.1	14.39
B	16	20	21	1	25.2	14.96
C	21	22	20	10	22.5	16.20
D	22	26	21	30	23.1	14.19

[a] γ_R is the regularization parameter. [b] Deviations defined as in Table 2.

that the spatial arrangement of the atoms of the solid in the CPG material may substantially differ from the arrangement that we have chosen to obtain the effective solid−fluid interaction potential, cf. section 3.2. However, as observed in Figure 6, introducing test variations in the values of ϵ_{sf} invariably leads to worse results. Thus we conclude that the solid−fluid potential depends essentially on the values of the molecular parameters ϵ_{sf} and σ_{sf} and not on the arrangement of the atoms at the solid wall, provided that the density is similar.

To summarize this section, we can conclude that the individual pore model can give good results for CPG if the appropriate pore geometry and molecular parameters are chosen. We have observed that the adsorption isotherms, obtained by weighting individual isotherms with the geometrical PSD of the CPG, are in better agreement with the overall isotherm of the material if slitlike, instead of cylindrical, pores are used in calculating the theoretical isotherm. However, the low-pressure regime is better described by the cylindrical geometry. The particular choice of the fluid−fluid and solid−fluid interaction parameters is less important than the pore geometry. Having checked that the molecular parameters are accurate and that the individual pore model is adequate for these materials, we proceed to check the capability of the procedure discussed in this paper in obtaining reliable PSDs by inversion of the adsorption integral.

5.2. PSD: Inversion of the Adsorption Integral. To validate our programs, the adsorption isotherms of material A reconstructed in the previous section from the geometrical PSD were used in eq 13, instead of the experimental adsorption isotherm, so that the theoretical adsorption isotherm is exact. The minimization of eq 13 then should exactly give the geometrical PSD as a solution. The parameter values used in these calculations and the deviation between adjusted isotherms are presented in Table 2. Results for cylinders are shown in Figure 7a, while Figure 7b shows the results for the case of slitlike pores. As observed in both figures, the calculated PSD ($f(H)$ in eq 13) is identical to the geometrical PSD of Gelb and Gubbins. Hence, the procedure is able to reproduce the physically relevant PSD.

As a further consistency check, we have not imposed the normalization condition in the minimization of eq 13. This is equivalent to leaving the porosity of the system as a free variable to be also obtained from the inversion procedure. Our calculations gave a porosity value very close to 30%, the same as that reported in ref 10.

With the above method, the adsorption integral equation was inverted for both geometries, cylindrical and planar,

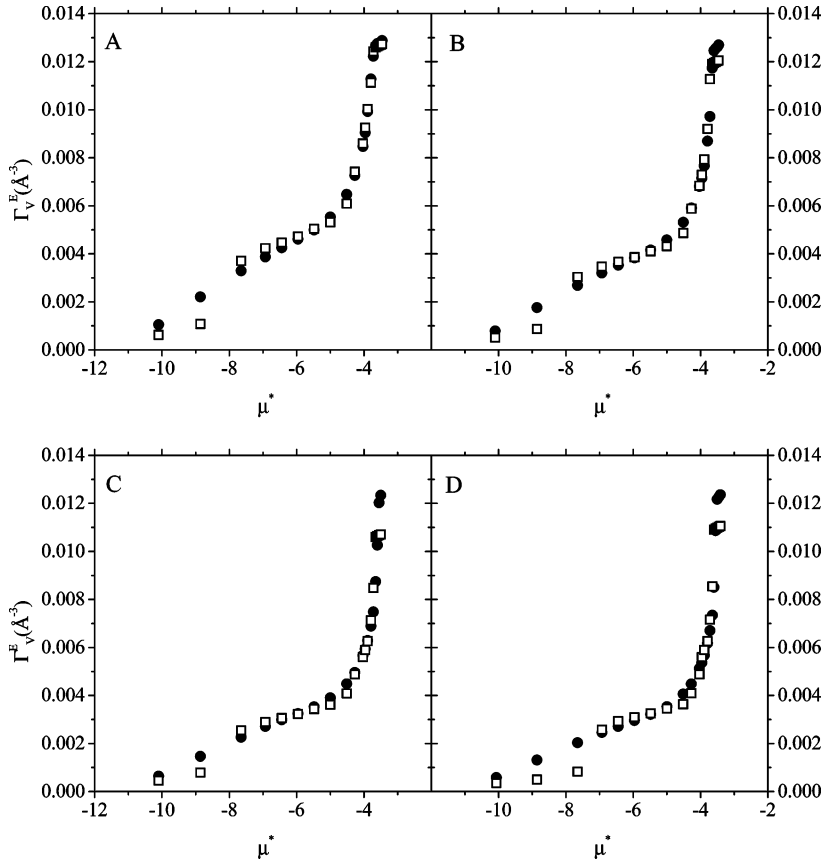

Figure 12. Adsorption isotherms obtained (squares) in this work using slitlike pores, including narrower sizes to solve eq 13, compared with experimental isotherms (circles) from ref 10 for each of the four systems A, B, C, and D.

and the results obtained were compared to those obtained by Gelb and Gubbins[10] with the BJH method and to the geometrical PSD. There is a discussion in the scientific community about which are the correct branches to be used to calculate PSDs, depending, among other facts, on the materials to be characterized. A recent work by Ravikovitch and Neimark[31] presents consistent PSD results for two different materials with both adsorption and desorption branches, also using two different gases. We have used here the adsorption branch of the isotherms for consistency with the work of Gelb and Gubbins.

The normalized PSDs obtained by minimizing eq 13 for each of the four materials using adsorption isotherms for cylindrical pores are shown in Figure 8 (open circles). Note that before normalizing, the area under the curve gives the factor which, multiplied by the experimental porosity $\mathscr{P}$, provides the estimated porosity from our method, $\mathscr{P}'$ (see Table 3). The resulting isotherms from the fitting are compared to the experimental isotherms in Figure 9. The percentage deviation for each fitting is given in Table 3. It is observed that the distributions obtained by inversion of the integral show, in general, better agreement with the geometrical distributions than those calculated with the BJH method. The locus of the peak is at the same pore size, except for material B, and they are all unimodal. The BJH distributions all show maxima systematically located at smaller pores than the actual one, and for materials A, B, and C, they show more than one peak. The discrepancies between the BJH results and the geometrical PSD were attributed to several factors.[10] One is that the BJH method follows the Kelvin equation, which is known to underestimate the pore size, especially for small pores.[1,44,45] An additional source of error may come from the use of the reference standard isotherm. It has been shown in a previous study[6] that the surface adsorption in very narrow pores is systematically higher than for a planar surface of identical characteristics. Finally, since the pores of these materials have an irregular geometry, with saddle points with negative curvature, a quantitative agreement should not be expected.

We observe in Figure 9 that the fitted adsorption isotherms of materials A and B lie above the experimental adsorption isotherms of the material at low pressures, while they are below the experimental isotherms in the condensation region, which reach a higher saturation level at pore filling. For materials C and D, we observe a very good agreement between fitted and "real" isotherms at low and moderate pressures, while the agreement deteriorates at high pressures. Since the independent pore model has been shown to be a rather good representation for these materials and since we have demonstrated that the regularization procedure is able to correctly reproduce the PSDs, the agreement should be better than what we obtain here. We conclude that the discrepancies may come from the fact that the cylindrical geometry is not the most appropriate to describe these materials, except for narrow pores. It should also be noted (see Table 3) that the regularization parameters needed are large, and the porosities obtained are lower than the 30% value provided by Gelb and Gubbins.

The normalized PSD obtained by inverting eq 13 using the slit pore model is also shown in Figure 8 for the four materials considered (filled circles). The parameters used, the calculated porosity before normalizing, and the

(44) Gregg, S. J.; Sing, K. S. W. *Adsorption, Surface Area and Porosity*, 2nd ed.; Academic Press: London, 1982; Chapter 3, p 132.

(45) Lastoskie, C.; Gubbins, K. E.; Quirke, N. *J. Phys. Chem.* **1993**, *97*, 4786.

percentage deviations are given in Table 4. The corresponding adsorption isotherms for the four materials are shown in Figure 10. The agreement between predicted isotherms and experimental ones is excellent, except in the very low pressure regime, corresponding to the adsorption in very narrow pores. In the PSDs, a clear improvement is observed in the location of the peaks in all cases. However, the distributions obtained are much broader than the geometrical ones, with a greater contribution of the narrow pore region. This decreases the contribution of the intermediate pores to the total isotherm, decreasing the adsorption in the high-pressure region, especially for materials C and D. The small values of the regularization parameter γ_R also suggest that this model is more descriptive of the actual material than the cylindrical pore model.

The open extreme at narrow pores of the PSDs may suggest the inclusion of narrower pores in the analysis. The normalized PSDs obtained by inverting eq 13 with two additional pores (diameters of 6 and 9 Å) for the slitlike geometry are presented in Figure 11, compared to the geometrical PSDs and those obtained without including these pores (Figure 8). The parameters used, the calculated porosity before normalizing, and the percentage deviations are given in Table 5. We did not perform the same analysis for the cylindrical case because the narrow pore extreme of the PSD was closed, indicating that the cylindrical pores included in calculating the PSD covered the whole range of relevant pore sizes for the adsorption of nitrogen in these materials. The new PSDs are very similar to the ones obtained before, except at the narrow pore extreme, where they begin to close, indicating the small contribution of narrower pores to the total PSD and hence to the adsorption behavior of the material. The corresponding adsorption isotherms for the four materials are shown in Figure 12. A comparison of this figure with Figure 10 shows an improvement of the overall adsorption at low pressures, while the agreement remains excellent at moderate and high pressures. This shows the importance of choosing a reliable range of pore sizes in order to calculate the PSD of adsorbent materials (see, for instance, ref 22 for a detailed discussion on the subject).

Therefore, we believe that the slit pore model seems to be a more appropriate model for these materials, except for very narrow pores. Although this may be a surprising result, looking at the structure of the material in the simulations of Gelb and Gubbins in ref 10, one can observe regions with locally concave and convex surfaces leading to an overall adsorption closer to that in an essentially slit geometry, better than in cylindrical geometry. At low pressures, the overall adsorption is better described by cylindrical pores, since at these pore sizes the curvature of the surfaces plays an essential role in adsorption.

6. Conclusions

We have applied the FMT in conjunction with a regularization method to estimate the PSD of model porous glasses. The way in which these model materials were "fabricated" allows one to geometrically measure the size and shape of the pores as well as the position of the atoms in the surface, making these glasses a good material with which to check the accuracy of characterization methods of porous materials available.

Since there are several solutions of the adsorption integral equation compatible with the experimental adsorption isotherm and several factors that can hide defects of the molecular model, or of the model material itself, we have made systematic studies of several aspects of the PSD fitting process. We have first checked the accuracy of the FMT and the independent pore model for predicting the experimental adsorption isotherms using the geometrical PSD already known for the materials. This has been done with individual cylindrical and slitlike pores. Second, once the adsorption isotherm was successfully reconstructed, we inverted the integral adsorption isotherm with a regularization procedure. The accuracy of the inversion method has also been checked before estimating the PSD of the different materials. Finally, once the method was validated, we used it to estimate the PSD of four materials by fitting to the experimental adsorption isotherms. We have also studied the influence of choosing different molecular parameters for the fluid−fluid and the solid−fluid interaction in the adsorption behavior of these systems.

We have shown that the independent pore model gives a good description of the adsorption isotherms for nitrogen, especially when the pores are represented as being of slit shape. The pore size distributions obtained using the independent pore model with DFT are in reasonable agreement with the exact geometrical PSDs for the Gelb/Gubbins model glasses. In particular, the PSD curves are unimodel and have a maximum at the same pore width as the exact PSDs. This is in contrast to the BJH method, which gives PSDs whose maxima are about 1 nm smaller than for the exact PSDs and gives a bimodal distribution in most cases. However, the PSDs from the independent pore model are broader than the exact ones, and the maximum is lower.

The finding that the slit pore geometry gives superior results to the cylinder model is surprising, but we believe this is due to the tortuosity of the pore structure. The material contains pores of different sizes, all interconnected, and there are opposite curvatures among them, making the overall *effective* curvature close to planar. However, at low pressures the adsorption is dominated by cylindrical pores.

We can finally conclude that the inversion methods based on the application of appropriate DFT techniques are a powerful tool to characterize real porous materials from the experimental knowledge of the adsorption isotherms. However, our analysis seems to indicate that the use of single pore geometry in the DFT calculations is not enough to reproduce the adsorption behavior in complex porous materials. Further insight on the properties of the adsorbent, like the tortuosity, for instance, can help in choosing the appropriate geometry for the pores. Furthermore, remaining discrepancies in the geometrical and inferred PSDs suggest that much work should be done to devise a reliable method to characterize porous materials.

Acknowledgment. We are thankful to Felipe J. Blas and Pedro Tarazona for helpful discussions. This work was supported by the Spanish Government, Ministerio de Ciencia y Tecnología (Grants No. PPQ2000-2888-E and PPQ2001-0671), and by the National Science Foundation of the USA (Grant No. CTS-0211792). S.F.-G. thanks URV (Spain) and CONACyT (México) for financial support.

LA034686V